

The Three Dimensional Structural Shape of the Gravitational Potential in the Local Group

Bomee Lee[†] and Joung hun Lee[†]

Department of Physics and Astronomy, FPRD, Seoul National University, Seoul 151-747, Korea

Accepted 2008 ??. Received 2008 ??. in original form 2007 October 10

ABSTRACT

The Local Group is a small galaxy cluster with the membership of 62 nearby galaxies including the Milky Way and M31. Although the Local Group has yet to be virialized, it interacts with the surrounding matter as one gravitationally bound system. To understand the formation and evolution of the Local Group as well as its member galaxies, it is important to reconstruct the gravitational potential field from the surrounding matter distribution in the local cosmic web. By measuring the anisotropy in the spatial distribution of the Local Group galaxies, which is assumed to be induced by the local gravitational tidal field, we resolve the three dimensional structure of the gravitational potential in the vicinity of the Milky Way smoothed on the Local Group mass scale. Our results show that (i) the minor principal axis of the Local Group tidal field is in the equatorial direction of $\alpha_p = 15^h 00^m$ and $\delta_p = 20^d$; (ii) it has a prolate shape with axial ratio of 0.5 ± 0.13 ; (iii) the global tides in the Local Group is quite strong, which may provide a partial explanation for the low abundance of dwarf galaxies in the Local Group.

Key words: methods:statistical – cosmology:theory – galaxies:clustering – galaxies:halos – large-scale structure of Universe

1 INTRODUCTION

Since Hubble (1936) first recognized its existence, the Local Group has been widely investigated by various observations (for a review, see Mateo 1998; Van den Bergh 2000, and references therein). It is now well known that the Local Group consists of two massive halos (the Milky Way and M31), their satellites, and the neighboring galaxies. It has been estimated by numerical simulations based on the disk formation model that the dark matter halos of the Milky Way and M31 have virial radius of approximately 200–300 kpc separated by about 700 kpc (Klypin et al. 2002; Widrow & Dubinski 2005). The comparison of the numerical results with observational constraints suggested that the Local Group is not yet relaxed with two main halos in the merging process.

Despite that the Local Group has yet to be virialized, it is also true that the Local Group behaves as one gravitationally bound system when interacting with the surrounding large-scale structure (e.g., Van den Bergh 2000). Therefore, to understand the formation and evolution of the Local Group under the gravitational influence from the surround-

ing matter distribution, it should be desirable to resolve the gravitational potential field around the Local Group.

As pointed out by Springel et al. (2004), it is the structure of the gravitational potential that reflects more directly the three dimensional distribution of dark matter in a given region. Recently, Hayashi et al. (2007) showed by numerical analysis of the N-body simulation results that the potential field is much smoother than the density field and the iso-potential surfaces are well approximated by concentric triaxial ellipsoids.

We attempt here to resolve the three dimensional structural shape of the gravitational potential in the regions around the Local Group, assuming that its iso-potential surfaces can be well approximated as a triaxial ellipsoid. To achieve this goal, we employ the analytic algorithm developed by Lee & Kang (2006, hereafter, LK06) which allows us to determine the eigenvalues of the tidal tensor (defined as the second derivative of the gravitational potential) from the anisotropic spatial distribution of the galaxies in a given cluster.

The underlying logic of the LK06 algorithm is as follows: The cluster galaxies are observed to be preferentially located near the major axes of the parent clusters (Knebe et al. 2004; Zentner et al. 2005). Recent numerical analyses based on N-body simulations have shown that this anisotropic dis-

[†] E-mail: bmlee@astro.snu.ac.kr

[†] E-mail: joung hun@astro.snu.ac.kr

tribution of the cluster galaxies originate from the local tidal field in the parent clusters (Atlay et al. 2006). What Lee & Kang (2006) found is that it is possible to determine the eigenvalues of the local tidal field by measuring the anisotropy in the spatial distribution of the cluster galaxies. Once the eigenvalues of the tidal field are determined, the axial ratios of the iso-potential surfaces can be readily calculated (Bardeen et al. 1986; Bond & Myers 1996).

The plan of this paper is as follows. In §2, the LK06 model is briefly overviewed and our theoretical formula based on the LK06 model is presented. In §3 the observational data are described and the anisotropy in the spatial distribution of the Local Group member galaxies is measured. Also the structural shape of the gravitational potential in the region around the Local Group is resolved. In §4 the results are discussed and a final conclusion is drawn.

2 THEORETICAL BACKGROUND

2.1 The gravitational potential profile

Let $\Phi(\mathbf{r})$ represent the gravitational potential field smoothed on the Local Group mass scale. In the neighborhood of the Local Group, the Taylor expansion gives

$$\Phi(\mathbf{r}) \approx \Phi(0) + r_i \partial_i \Phi|_0 + \frac{1}{2} r_i r_j \partial_i \partial_j \Phi|_0, \quad (1)$$

where it is assumed that the center of the mass of the Local Group is positioned at the origin of $\mathbf{r} = 0$. Supposing that the Local Group represents a local peak of the smoothed potential field, the second term proportional to $\partial_i \Phi|_0$ in equation (1) becomes zero. The tidal shear tensor \mathbf{T} in the Local Group is defined as $T_{ij} \equiv \partial_i \partial_j \Phi|_0$ at the local peak to which the third term in equation (1) is proportional.

In the frame of the principal axes of the tidal shear tensor, equation (1) can be expressed as

$$\Phi(\mathbf{r}) - \Phi(0) \approx \frac{1}{2} r_i^2 \lambda_i, \quad (2)$$

where, $\lambda_1, \lambda_2, \lambda_3$ are the eigenvalues of \mathbf{T} with $\lambda_1 \geq \lambda_2 \geq \lambda_3$. Let a_1, a_2, a_3 be the three semi-axes of an ellipsoidal iso-potential surface of $\Phi(\mathbf{r}) = \text{const.} \equiv \phi$. By equation (2), one can relate $\{a_i\}_i^3$ to $\{\lambda_i\}_i^3$ as

$$a_i = \left[\frac{2(\Phi(0) - \phi)}{\lambda_i} \right]^{1/2}. \quad (3)$$

Therefore, the two axial ratios of the ellipsoidal iso-potential surfaces can be written only in terms of $\{\lambda_i\}_i^3$ as

$$\frac{a_1}{a_3} = \sqrt{\frac{\lambda_3}{\lambda_1}}, \quad \frac{a_2}{a_3} = \sqrt{\frac{\lambda_3}{\lambda_2}}. \quad (4)$$

Equation (4) implies that once the eigenvalues of the tidal shear tensor at the Local Group region are determined, the three dimensional shape of the Local Group potential can be reconstructed.

2.2 Overview of the LK06 algorithm

Assuming that the tidal field in the host halo is responsible for the anisotropic spatial distribution of the substructures, Lee & Kang (2006) have derived an analytic expression for

the probability distribution of the cosines of the polar angles of the substructure position vectors in the tidal shear principal axis frame as

$$p(\cos \theta) = \frac{1}{2\pi} \prod_{i=1}^3 (1 - s + 3s\hat{\lambda}_i^2)^{-1/2} \times \int_0^{2\pi} \left(\frac{\sin^2 \theta \cos^2 \phi}{1-s+3s\hat{\lambda}_1^2} + \frac{\sin^2 \theta \sin^2 \phi}{1-s+3s\hat{\lambda}_2^2} + \frac{\cos^2 \theta}{1-s+3s\hat{\lambda}_3^2} \right)^{-3/2} d\phi, \quad (5)$$

where s is a correlation parameter in the range of $[-1, 1]$ and $\{\hat{\lambda}_i\}_{i=1}^3$ are the unit eigenvalues of \mathbf{T} satisfying the constraint of $\hat{\lambda}_1^2 + \hat{\lambda}_2^2 + \hat{\lambda}_3^2 = 1$. Here, the free parameter s quantifies the degree of the alignment between the minor principal axis of the tidal tensor and the position vectors of the substructures: If $s = -1$, then the substructures are most strongly aligned with the minor principal axis of the tidal tensor; If $s = 1$, they are most strongly anti-aligned while the case of $s = 0$ corresponds to no alignment.

Since the minor principal axis of the tidal tensor at the region of a given host halo corresponds to the direction in which the tidal force is least strong and thus the host halo is most elongated, Lee & Kang (2006) assumed that the minor principal axis of the tidal tensor is parallel to the major principal axis of the inertia tensor of the host halo. Under this assumption, they suggested that by measuring $p(\cos \theta)$ from the spatial distribution of the substructure positions and fitting it to equation (5), one can determine the unit eigenvalues of the tidal tensor and the value of the correlation parameter, which will in turn yield the values of the axial ratios of the host halo. To demonstrate the validity of their algorithm, Lee & Kang (2006) tested it against N-body results, and showed that their algorithm indeed reconstruct the actual shapes of cluster halos within 20% error.

In the original approach, Lee & Kang (2006) used the virialization constraint of $\sum_i^3 \lambda_i = \delta_c$ where $\delta_c \approx 1.68$ is the density threshold for a virialized structure (Eke et al. 1996). However, note that the LK06 algorithm can be applied even to a region that is not completely virialized, since the virialization condition was not used to derived equation (5) itself. In fact, it can be applied to any region as long as the member objects in the region show tidally induced anisotropy. For instance, it can be used to describe the anisotropic spatial distribution of galaxy clusters in the superclusters due to the supercluster tidal field (i.e., the linear tidal field smoothed on the supercluster mass scale), even though the superclusters are not virialized objects (Lee & Evrard 2007). It has been also used to describe the anisotropic spatial distribution of void galaxies due to the tidal effect from the surrounding filaments even though the voids are obviously not virialized (Lee & Park 2006).

When the LK06 algorithm is applied to an unvirialized structure, the additional constraint of $\sum_i^3 \lambda_i = \delta_c$ should not be used. Therefore, what one can reconstruct by the LK06 algorithm for this case is not the shape defined by the inertia momentum tensor of the structure but the shape of the potential around the structure. In the following section, we reconstruct the three dimensional structural shape of the gravitational potential in the region around the Local Group by measuring the values of s and $\{\hat{\lambda}_i\}_{i=1}^3$ from recent observational data.

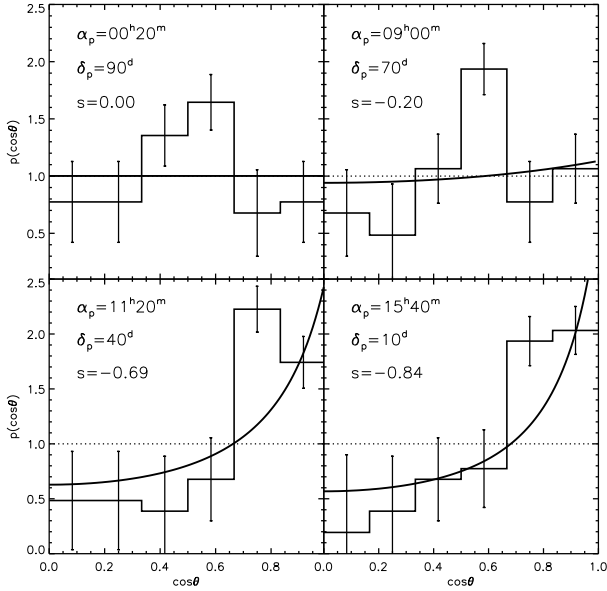


Figure 1. Probability density distribution of the cosines of the angles between the position vectors of the Local Group member galaxies in the CL frame and four different choices of major principal axis of the Local Group. In each panel, the histogram with Poisson errors represents the observational data points of Local Group, the solid line is the analytic fitting from LK06 reconstructing algorithm, and the dotted line corresponds to the case of no correlation. Four plots in each panel show how the agreements between the observational and the analytic results change if different directions are used rather than the major principal axis.

3 APPLICATION TO THE LOCAL GROUP DATA

3.1 Tidal Alignment of the Local Group

We use the observational data of 62 member galaxies belonged to the Local Group. Table 1 lists the latest information on the equatorial coordinate (α, δ) , distance (r) in unit of Mpc and absolute magnitude (M_v) of each member galaxy. The information on α , δ , r and M_v for the #1 – 40 and #48 galaxies are obtained from Karachentsev et al. (2004), and for the other galaxies, we show in the seventh columns the references from which we obtained the information. For those galaxies marked by \star in Table 1 we used the updated information given in McConnachie et al. (2005). Since the mass information is not available, we calculate the center-of-luminosity (CL) instead of the center-of-mass (CM) for the Local Group by using the information on the absolute magnitude of each member galaxies. The Cartesian position of the Local Group CL in the equatorial coordinate system is found to be $\text{CL} = [0.351, 0.069, 0.259]$ in unit of Mpc.

We measure the three dimensional positions of the Local Group member galaxies in the CL frame in the equatorial coordinates. Then, we attempt to find a direction in the equatorial coordinates, say, α_p and δ_p , with which the position vectors of the Local Group member galaxies in the CL frame show the highest degree of anisotropy. We will re-

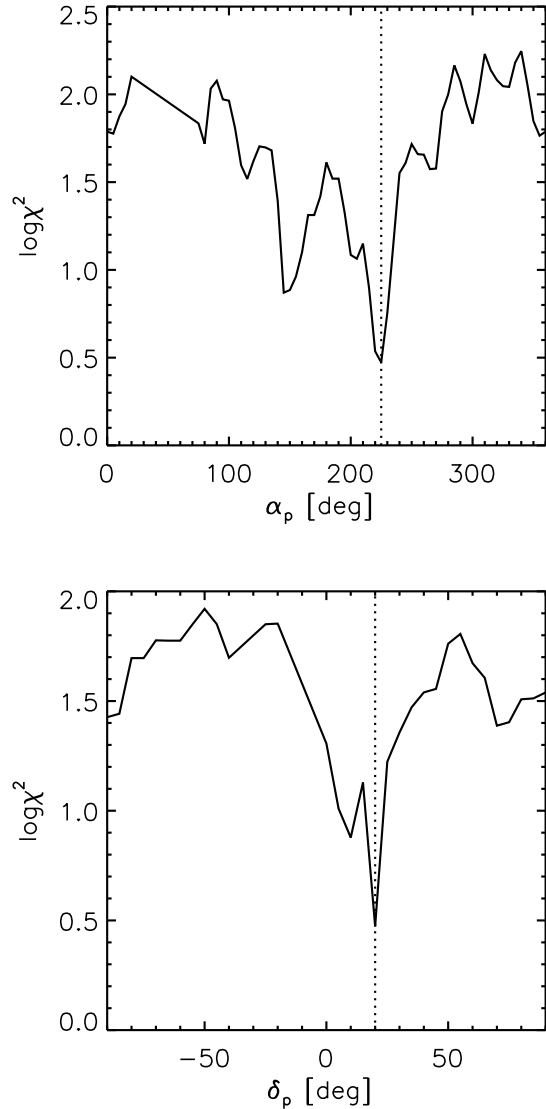


Figure 2. The variation of χ^2 as a function of α_p (top) and δ_p (bottom) when the other parameters are fixed at the best-fit values. In each panel the vertical dotted line indicates the position at which χ^2 has the minimum value ($\alpha_p = 225^\circ$, $\delta_p = 20^\circ$).

gard this direction, if found, as the direction of the minor principal axis of the local tidal field.

Let θ represent the angle between the equatorial position vector of a given member galaxy and the direction of (α_p, δ_p) . Changing the values of α_p and δ_p by 5° systematically from 0° to 360° and -90° to 90° , respectively, we measure repeatedly the probability distribution, $p(\cos \theta)$, and search for (α_p, δ_p) which leads to the maximum deviation of $p(\cos \theta)$ from uniform distribution. The bin size of 5° is chosen as the smallest bin size below which the numerical noise dominate. By fitting equation (5) to the observational results, we determine a direction of (α_p, δ_p) which leads the maximum deviation of $p(\cos \theta)$ from uniform distribution.

Fig. 1 plots the cases of four different directions of the minor principal axis of the Local Group tidal field as exam-

Table 1. Observational Data on the Local Group

No	Name	α (2000) [$h:m:s$]	δ (2000) [$d:m:s$]	r [Mpc]	M_v	Reference
1	WLM	00 01 58.1	-15 27 40	0.932 *	-14.4	
2	NGC55	00 08 13.3	-34 13 13	1.80	-17.5	
3	IC 10	00 20 24.5	59 17 30	0.66	-10.1	
4	NGC147	00 33 11.6	48 30 28	0.675 *	-15.1	
5	And III	00 35 33.8	36 29 52	0.749 *	-10.2	
6	NGC 185	00 38 58	48 20 10	0.616 *	-15.6	
7	NGC 205	00 40 22.5	41 41 11	0.824 *	-16.4	
8	M32	00 42 42.1	40 51 59	0.77	-16.5	
9	M31	00 42 44.5	41 16 09	0.785 *	-21.2	
10	And I	00 45 40	38 02 14	0.745 *	-11.8	
11	SMC	00 52 38	-72 48 01	0.06	-17.1	
12	Sculptor	01 00 09.4	-33 42 33	0.09	-9.8	
13	LGS 3	01 03 56.6	21 53 41	0.769 *	-10.4	
14	IC 1613	01 04 54.10	02 07 60	0.73	-15.3	
15	And II	01 16 29.8	33 25 09	0.652 *	-9.1	
16	M33	01 33 50.8	30 39 37	0.809 *	-18.9	
17	Phoenix	01 51 06.3	-44 26 41	0.44	-9.8	
18	Fornax	02 39 54.7	-34 31 33	0.14	-13.1	
19	EGB 0427+63	04 32 00.3	63 36 50	1.80	-15.9	
20	LMC	05 23 34.6	-69 45 22	0.05	-18.5	
21	Carina	06 41 36.7	-50 57 58	0.10	-9.4	
22	Leo A	09 59 26.4	30 44 47	0.69	-11.5	
23	Sextans B	10 00 00.1	05 19 56	1.36	-14.0	
24	NGC 3109	10 03 07.2	-26 09 36	1.33	-15.5	
25	Antlia	10 04 04	-27 19 55	1.32	-9.8	
26	Leo I	10 08 26.9	12 18 29	0.25	-11.9	
27	Sextans A	10 11 00.8	-04 41 34	1.32	-13.9	
28	Sextans	10 13 03	-01 36 52	0.09	-9.5	
29	Leo II	11 13 29.2	22 09 17	0.21	-10.1	
30	GR 8	12 58 40.4	14 13 03	2.10	-12.0	
31	Ursa Minor	15 09 11.3	67 12 52	0.06	-8.9	
32	Draco	17 20 01.4	57 54 34	0.08	-8.6	
33	Milky Way	17 45 09.2	-28 01 12	0.01	-20.9	
34	Sagittarius	18 55 03.1	-30 28 42	0.02	-13.8	
35	SagDIG	19 29 59	-17 40 41	1.04	-12.0	
36	NGC 6822	19 44 57.7	-14 48 11	0.50	-16.0	
37	Aquarius	20 46 51.8	-12 50 53	1.071*	-10.9	
38	IC 5152	22 02 41.9	-51 17 43	2.07	-15.6	
39	Tucana	22 41 49	-64 25 12	0.88	-9.6	
40	UKS 2323-326	23 26 27.5	-32 23 26	2.23	-12.9	
41	Pegasus	23 28 34.1	14 44 48	0.919*	-12.3	Mateo (1998)
42	And VII	23 26 31.8	+50 40 32	0.763*	-13.3	Van den Bergh (2000)
43	And VI	23 51 46.4	+24 35 10	0.82	-11.5	Whiting et al. (2007)
44	Cetus	00 26 11.0	-11 02 40	0.755*	-11.3	Whiting et al. (1999)
45	And V	01 10 17.1	+47 37 41	0.774*	-9.6	Van den Bergh (2000)
46	And IX	00 52 52.8	+44 12 00	0.765*	-8.3	Zucker et al. (2004)
47	Canis Major dwarf	07 12 36	-27 40 00	0.008	-	Martin et al. (2004)
48	Cas1	02 06 07.9	+69 00 36	3.3	-15.6	
49	Bootes dwarf	14 00 06	+14 30 00	0.06	-5.8	Belokurov et al. (2006)
50	Canes Ven atici	13 28 03.5	+33 33 21	0.22	-7.9	Zucker et al. (2006a)
51	Willman1	10 19 22	+51 03 03	0.045	-3.0	Willman et al. (2005b)
52	Ursa Major	10 34 53	+51 55 12	0.1	-6.75	Willman et al. (2005a)
53	Ursa Major II	08 51 30	+63 07 48	0.032	-3.8	Zucker et al. (2006b)
54	Heracles	11 32 57	-00 32 00	0.16	-5.1	Belokurov et al. (2007)
55	Coma Berenices	12 26 59	+23 54 15	0.044	-3.7	Belokurov et al. (2007)
56	Segue1	10 07 04	+16 04 55	0.023	-3.0	Belokurov et al. (2007)
57	Leo IV	16 31 02	+12 47 30	0.14	-6.0	Belokurov et al. (2007)
58	And X	01 06 33.7	+44 48 15.8	0.7	-8.1	Zucker et al. (2007)

59	Canes Venatici II	12 57 10	+34 19 15	0.15	-4.8	Belokurov et al. (2007)
60	Bootes II	13 58 00	+12 51 00	0.06	-	Walsh et al. (2007)
61	Leo T	09 34 53.4	+17 03 05	0.42	-7.2	Ryan-Weber et al. (2008)
62	And XVII	00 37 07	+44 19 20	0.794	-8.5	Irwin et al. (2008)

References: No.1 ~ 40 and 48 from Karachentsev et al. (2004); * McConnachie et al. (2005)

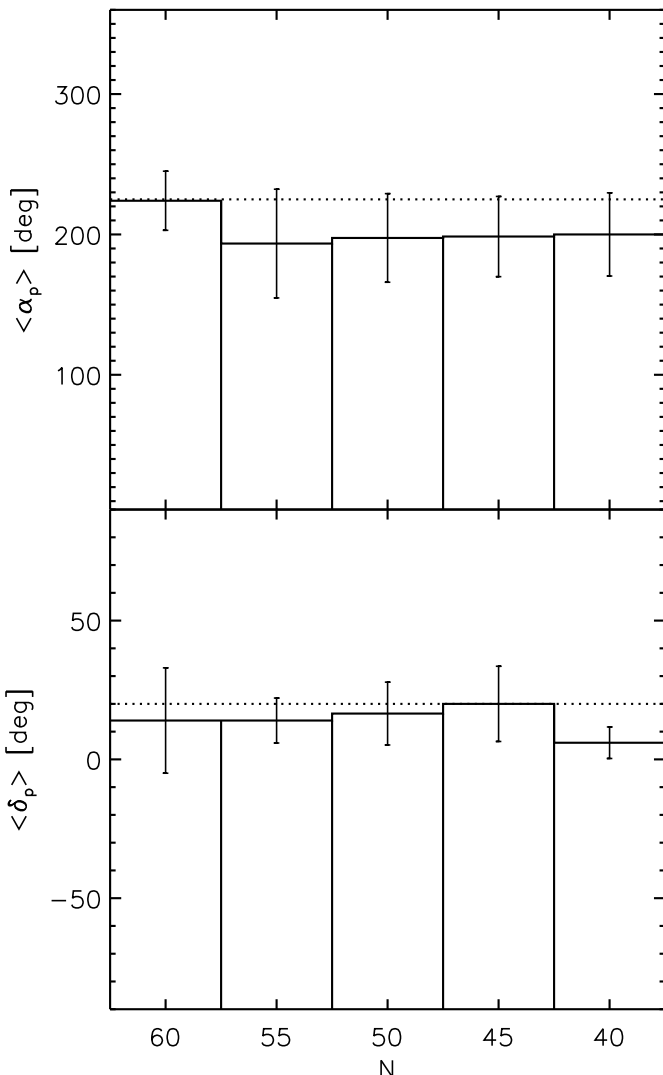


Figure 3. The mean values, $\langle \alpha_p \rangle$ (top) and $\langle \delta_p \rangle$ (bottom), averaged over 10 samples of N randomly selected galaxies out of the 62 Local Group members. In each panel the errors represent one standard deviation between samples and the horizontal dotted line correspond to our result of $(\alpha_p = 225^\circ, \delta_p = 20^\circ)$.

plexes. In each panel, the histogram with Poisson errors corresponds to the observational results while the solid curve is the fitting model (eq.[5]) with the best-fit values of $\hat{\lambda}_1$, $\hat{\lambda}_2$ and s : For a given direction of (α_p, δ_p) , we fit equation (5) to the observational result of $p(\cos \theta)$ by adjusting the values of $\hat{\lambda}_1$, $\hat{\lambda}_2$, and s and determine for the best-fit values of the three parameters with the help of the χ^2 statistics. As can be seen in Fig. 1, the observed distribution of $p(\cos \theta)$ behaves quite differently as the direction of (α_p, δ_p) changes. For a certain direction of (α_p, δ_p) , the distribution becomes quite uniform (top-left). While for another direction $p(\cos \theta)$

increases sharply with $(\cos \theta)$ indicating preferential alignments of the galaxy's position vectors with the given directions and the analytic fits work well (bottom-right).

It is found that the direction of $(\alpha_p = 15^\circ 00^m, \delta_p = 20^d)$ leads to the maximum alignments. In other words, when this direction is chosen as the minor principal axis of the Local Group tidal field, equation (5) agrees with the observational results best with the value of χ^2 minimized. Fig. 2 plots χ^2 as a function of α_p (top) and δ_p (bottom) when the three other parameters are fixed at their best-fit values. In each panel the vertical dotted line indicates the position at which χ^2 has the minimum value. It is worth mentioning here that the direction we found as the minor principal axis of the Local Group tidal field ($\alpha = 15^\circ 00^m, \delta = 20^d$) does not coincide with the direction parallel to the connection line between M31 and MW. It indicates that the observed anisotropic distribution of the LG galaxies is induced by the tidal effect of the surrounding matter distribution not by the fact that the majority of them are the satellites of M31 and MW.

To examine how stable our result is, we construct 10 samples of N randomly selected galaxies out of the parent sample of 62 members. For each sample, we determine the best-fit values of α_p and δ_p using the same procedure described in the above, and calculate the means of α_p and δ_p averaged over 10 samples. Fig. 3 plots $\langle \alpha_p \rangle$ and $\langle \delta_p \rangle$ as a function of N as histogram in the top and bottom panel, respectively. In each panel the errors represent one standard deviation between samples and the horizontal dotted line represents our best-fit result ($\alpha_p = 225^\circ, \delta_p = 20^\circ$), obtained from the 62 LG galaxies. As can be seen, the variations of $\langle \alpha_p \rangle$ and $\langle \delta_p \rangle$ with N stay within one standard deviation, until the value of N decreases down to 45. At the bin of $N = 40$, however, $\langle \delta_p \rangle$ suddenly drops by more than two standard deviations. Therefore, one can say that our result is stable as long as more than 45 LG galaxies are used to reconstruct the minor principal axis of the tidal field.

Since the effect of the nonlinear process like merging between MW and M31 should be dominant near the LG center, the spatial distribution of those galaxies located near the LG center like the satellites of the MW and M31 are not good indicators of the tidal effect. Only when a large fraction of distant member galaxies whose positions are not severely modified by the merging effect are included, the overall spatial distribution of the LG member galaxies will reveal the anisotropy induced by the local tidal effect.

When the minor principal axis of the Local Group tidal field is determined as this direction, the values of the fitting parameters are found to be $\hat{\lambda}_1 = 0.7 \pm 0.04$, $\hat{\lambda}_2 = 0.69 \pm 0.04$ and $s = -0.99 \pm 0.27$. Note that this corresponds to the unit eigenvalues of the tidal field smoothed on the Local Group mass scale. Fig. 5 compares this best-fit model (solid line) with the observational result (dots) with Poisson errors for the minor axis direction of $(\alpha_p = 15^\circ 00^m, \delta_p = 20^d)$. As can be seen, the fitting model agrees with the observational

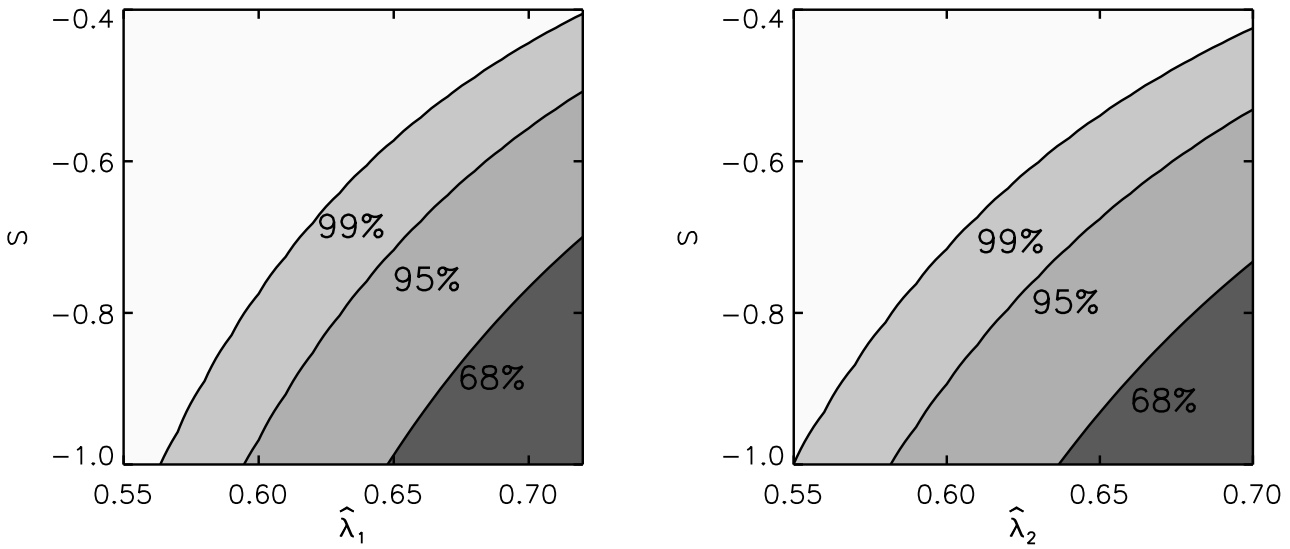


Figure 4. 68%, 95% and 99% contour plots for s and $\hat{\lambda}_1$ (left) and for s and $\hat{\lambda}_2$ (right). In each panel the other parameter is fixed at its best-fit value.

result pretty well. The probability distribution of $p(\cos\theta)$ with the best-fit parameters indeed shows strong alignments between the minor axis of the Local Group tidal field and the positions of the Local Group galaxies.

The unmarginalized error in the measurements of the best-fit values of $\hat{\lambda}_1$, $\hat{\lambda}_2$ and s are calculated by using the formula given in (Bevington & Robinson 1996). For instance, the error in the measurement of $\hat{\lambda}_1$ is calculated as

$$\sigma_{\hat{\lambda}_1} = \Delta\hat{\lambda}_1 \sqrt{2(\chi_1^2 - 2\chi_2^2 + \chi_3^2)^{-1}}. \quad (6)$$

where $\Delta\hat{\lambda}_1$ is the bin size of $\hat{\lambda}_1$. Here, $\chi_i^2 = \chi^2(\hat{\lambda}_{1i})|_{i=1,2,3}$ and $\hat{\lambda}_{12} = \hat{\lambda}_{11} + \Delta\hat{\lambda}_1$, $\hat{\lambda}_{13} = \hat{\lambda}_{12} + \Delta\hat{\lambda}_1$ and $\hat{\lambda}_{11}$ is the best-fit value. The error associated with the best-fit values of $\hat{\lambda}_1$ and s are also calculated in a similar manner. To account for the parameter degeneracy and estimate the marginalized errors in the measurement of the best-fit values, we also compute the 68%, 95% and 99% confidence regions for $(s, \hat{\lambda}_1)$ and for $(s, \hat{\lambda}_2)$, which are shown in the left and right panels of Fig. 4, respectively.

By expressing equation (4) in terms of the unit eigenvalues, we can now measures the three dimensional shape of the gravitational potential in the region around the Local Group:

$$a_1/a_3 = \sqrt{\frac{\hat{\lambda}_3}{\hat{\lambda}_1}}, \quad a_2/a_3 = \sqrt{\frac{\hat{\lambda}_3}{\hat{\lambda}_2}}. \quad (7)$$

The axial ratios of the ellipsoidal iso-potential surfaces are calculated as $a_1/a_3 = 0.51 \pm 0.13$ and $a_2/a_3 = 0.52 \pm 0.13$. The associated errors are estimated by means of the error propagation method (Bevington & Robinson 1996) as

$$\sigma_f^2 = \sigma_{\hat{\lambda}_1}^2 \left(\frac{\partial f}{\partial \hat{\lambda}_1} \right)^2 + \sigma_{\hat{\lambda}_2}^2 \left(\frac{\partial f}{\partial \hat{\lambda}_2} \right)^2 \quad (8)$$

where f represents the two axial ratios. Our results indicate

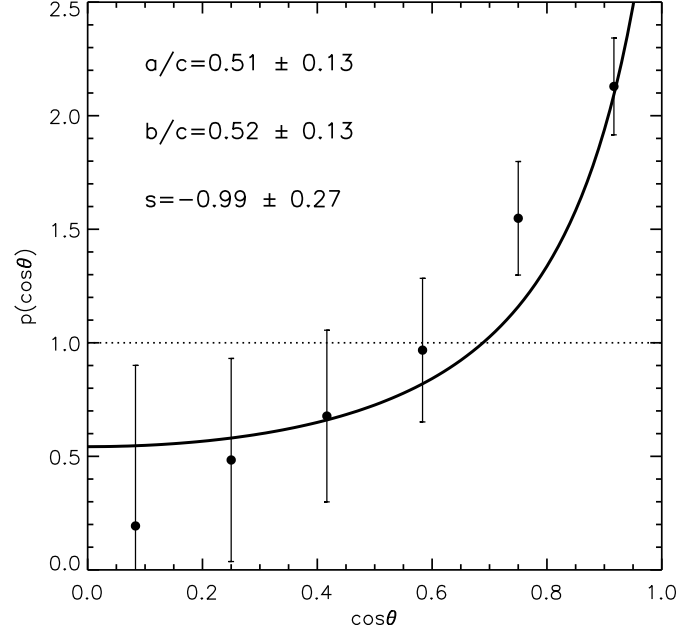


Figure 5. Probability distribution of the cosines of the angles between the spatial positions of the Local Group member galaxies and the major principal axis, $\alpha = 15^h 00^m$, $\delta = 20^d$. The solid line corresponds to the fitting model (eq.[5]) with the best-fit parameters of $s = -0.99$ and $a_1/a_3 = 0.51$, $a_2/a_3 = 0.52$ while the solid dots with Poisson errors represent the observational results.

that the gravitational potential in the Local Group has a prolate shape. Figure 5 plots our final result.

3.2 Strength of the Tidal Effect in the Local Group

Now that we have determined the unit eigenvalues of the tidal shear field in the region around the Local Group, we can estimate the strength of the global tides in the Local Group. Since the global tides plays a role of stripping or destroying the substructures, if it is found to be strong in the Local Group, then it might explain at least partially the low abundance of member galaxies in the Local Group.

The degree of the tidal effect can be quantified in terms of the differences between the three eigenvalues of the tidal tensor as (Chiueh & Lee 2001)

$$\hat{\Lambda}_T = \sqrt{\frac{1}{3}[(\hat{\lambda}_1 - \hat{\lambda}_2)^2 + (\hat{\lambda}_2 - \hat{\lambda}_3)^2 + (\hat{\lambda}_1 - \hat{\lambda}_3)^2]}. \quad (9)$$

Here the value of $\hat{\Lambda}_T$ is in the range of $[0, 1]$. The case of $\hat{\Lambda}_T = 0$ corresponds to no tidal effect. The higher the degree of the deviation of $\hat{\Lambda}_T$ from zero is, the stronger the tidal effect is. It is found that $\hat{\Lambda}_T = 0.42$ for the Local Group from the best-fit values of $\hat{\lambda}_1$ and $\hat{\lambda}_2$ obtained in §3.1, which suggests that the global tides in the Local Group is quite strong.

4 DISCUSSION AND CONCLUSION

We have shown here that the anisotropic spatial distribution of the Local Group galaxies can be used to reconstruct by means of the LK06 algorithm the shape of the gravitational potential in the vicinity of the MW smoothed on the Local Group mass scale and measure the strength of the tidal effect, which is important to understand the interaction of the Local Group as a whole with the surrounding matter distribution and its evolution.

In their original approach, Lee & Kang (2006) reconstructed the ellipsoidal shape of the host halos rather than the gravitational potential from the anisotropic spatial distribution of the halo substructures by using the Zel'dovich approximation (Zel'dovich 1970) as well as the virialization condition. We did not apply their original approach to the Local Group since the Local Group has yet to be completely virialized (Klypin et al. 2002; Widrow & Dubinski 2005).

Nevertheless, the LK06 algorithm can in fact apply to any overdense region in which the embedded structures show anisotropic spatial distribution since it has not been derived under a virialization condition. For example, Lee & Evrard (2007) used the LK06 algorithm to reconstruct the filamentary shapes of the superclusters by measuring the cluster-supercluster alignments even though the superclusters are not completely relaxed systems. For the case of unrelaxed systems, however, what can be reconstructed by the LK06 algorithm is the anisotropy in the gravitational potential but not the shape of a bound halo.

Here, we have reconstructed the anisotropy in the gravitational potential around the Local Group from the spatial distribution of the Local Group galaxies. It is shown that the Local Group potential is prolate with axial ratios of 0.5 ± 0.13 with the major principal axis parallel to the direction of the equatorial coordinate, $\alpha = 15^h 00^m$, $\delta = 20^d$. Even though our result still suffers from large errors due to small number statistic, it has been obtained without resorting to any ad-

ditional assumption on the dynamical state or the shape of the Local Group.

It is worth discussing one caveat that our result is subject to. As mentioned in Section 3.1, the reconstruction procedure is stable as long as more than 40 galaxies of the Local Group are used. We think that this caveat comes from the radial dependence of the final result. Since the effect of such nonlinear process as gravitational merging and interaction between the MW and the M31 should be dominant in the inner region of the Local Group, the spatial distribution of those nearby galaxies like the satellites of the MW and M31 should not be good indicators of the tidal effect.

Meanwhile the positions of the distant galaxies located in the outer region of the Local Group are not severely modified by the nonlinear effect and thus their spatial distribution will reflect better the effect of the Local Group tidal field. It would be desirable to investigate how the triaxial structure of the Local Group potential changes with radial distance. It is, however, beyond the scope of this paper since the total number of the Local Group member galaxies is too small to obtain reliable statistical result on the radial dependence. We plan to apply the LK06 algorithm to the Virgo cluster and investigate the radial dependence of the Virgo cluster potential shape, given the fact that the Virgo cluster has much more member galaxies than the Local Group. We wish to report the result in the near future.

From the measured eigenvalues of the tidal tensor, we have also shown that the the global tides are quite strong in the current Local Group system, which may provide an explanation to the low abundance of dwarf galaxies in the Local Group (somerville 2002): In the Local Group system where the two main galaxies are in the process of filamentary merging the low-mass dwarf galaxies are hard to survive due to the strong global tides. An interesting question to ask is what the critical mass of the member galaxy is to survive the global tides in the Local Group? We also intend to work on this issue in the future.

ACKNOWLEDGMENTS

We are very grateful to A. Knebe for his very useful referee report which helped us improve the original manuscript significantly. We acknowledge the Korea Science and Engineering Foundation (KOSEF) grant funded by the Korean Government (MOST,NO. R01-2007-000-10246-0).

REFERENCES

- Atlay G., Colberg J. M., Croft R. A. C., 2006, MNRAS, 1422, 1428
- Bardeen J. M., Bond J. R., Kaiser N., Szalay, A. S., 1986, ApJ, 304, 15
- Belokurov, V., et al., 2006, ApJ, 647, L111
- Belokurov, V., et al., 2007, ApJ, 654, 897
- Bevington P. R., Robinson D. K., 1996, Data Reduction and Error Analysis for the Physical Sciences (Boston : McGraw-Hill)
- Bond J. R., Myers, 1996, ApJS, 103, 1
- Chiueh T., Lee J., 2001, APJ, 555, 83
- Eke V. R., Cole S., Frenk C. S., 1996, MNRAS, 282, 263

8 *Bomee Lee and Joungjun Lee*

Hayashi E., Navarro J. F., & Springel V., 2007, MNRAS, 377, 50

Hubble E., 1936, The Realm of the Nebulae (Yal Univ. Press)

Irwin, M. J., Ferguson, A. M. N., Huxor, A. P., Tanvir, N. R., Ibata, R. A., & Lewis, G. F. 2008, ApJ, 676, L17

Kang X., Mao S., Gao L., Jing Y. P., 2005, A& A, 437, 383

Karachentsev I. D., Karachentseva V. E., Huchtmeier W. K., Makarov D. I., 2004, AJ, 127, 2031

Martin, N. F., Ibata, R. A., Bellazzini, M., Irwin, M. J., Lewis, G. F., & Dehnen, W., 2004, MNRAS, 348, 12

McConnachie, A. W., Irwin, M. J., Ferguson, A. M. N., Ibata, R. A., Lewis, G. F., & Tanvir, N., 2005, MNRAS, 356, 979

Kitayama T., Suto Y., 1996, APJ, 469, 480

Klypin A., Zhao H. S., Somerville, R. S., 2004, ApJ, 573, 597

Knebe, A. et al. 2004, ApJ, 603, 7

Lee J., Pen U. L., 2000, ApJ, 532, L5

Lee J., Pen U. L., 2001, ApJ, 555, 106

Lee J., Jing Y. P., Suto Y., 2005, APJ, 632, 706

Lee J., Kang X., 2006, ApJ, 637, 561

Lee J., Park D, 2006, ApJ, 652,1

Lee J., Evrard A.E., 2007, APJ, 657, 30

Libeskind N. I., Frenk C. S., Cole S., Helly J. C., Jenkins A., Navarro J. F., Power C., 2005, MNRAS, 363, 146

Mateo Mario, 1998, ARA& A, 36, 435M

Peñarrubia, J., McConnachie, A. W., & Navarro, J. F., 2008, ApJ, 672, 904

Ryan-Weber, E. V., Begum, A., Oosterloo, T., Pal, S., Irwin, M. J., Belokurov, V., Evans, N. W., & Zucker, D. B., 2008, MNRAS, 384, 535

Somerville R. S., 2002, ApJ, 572, L23

Springel V., White S. D. M., Hernquist L., 2004, in Ryder S., Pisano D., Walker M., Freeman K., eds, Proc. IAU Symp. 220, the Shapes of Simulated Dark Matter Haloes. Astron. Soc. Pac., San Francisco, p. 421

Walsh, S. M., Jerjen, H., & Willman, B., 2007, ApJ, 662, L83

West M. J., 1989, ApJ, 347, 610

Widrow L. M., & Dubinski J. 2005, ApJ, 631, 838

Whiting, A. B., Hau, G. K. T., & Irwin, M., 1999, AJ, 118, 2767

Whiting A. B. Hau, G. K. T., Irwin, M., & Verdugo, M., 2007, AJ, 133, 715

Willman, B., et al., 2005, ApJ, 626, L85

Willman, B., et al., 2005, AJ, 129, 2692

Van den Bergh S., 2000, PASP, 112, 529

Zel'dovich Y. B., 1970, A& A, 5, 84

Zentner A. R., Kravtsov A. V., Gnedin, O. Y., Klypin, 2005, ApJ, 629, 219

Zucker, D. B., et al., 2004, ApJ, 612, L121

Zucker, D. B., et al., 2006, ApJ, 643, L103

Zucker, D. B., et al., 2006, ApJ, 650, L41

Zucker, D. B., et al., 2007, ApJ, 659, L21